crystals

MDPI

Article

Facet Appearance on the Lateral Face of Sapphire Single-Crystal Fibers during LHPG Growth

Liudmila D. Iskhakova [1], Vitalii V. Kashin [2], Sergey V. Lavrishchev [1], Sergey Ya. Rusanov [2], Vladimir F. Seregin [2] and Vladimir B. Tsvetkov [2,3,*]

1 Fiber Optics Research Center of the Russian Academy of Sciences, Vavilov Str., 38, 119333 Moscow, Russia; ldisk@fo.gpi.ru (L.D.I.); lavr@fo.gpi.ru (S.V.L.)

2 A.M. Prokhorov General Physics Institute, Russian Academy of Sciences, Vavilov Str., 38, 119991 Moscow, Russia; kashin@lsk.gpi.ru (V.V.K.); s.rusanov@kapella.gpi.ru (S.Y.R.); seregin@lsk.gpi.ru (V.F.S.)

3 National Research Nuclear University MEPhI, Kashirskoe sh., 31, 115409 Moscow, Russia

* Correspondence: tsvetkov@lsk.gpi.ru; Tel.: +7-499-503-8390

Academic Editor: Ekaterina Pomjakushina

Received: 31 May 2016; Accepted: 28 July 2016; Published: 25 August 2016

Abstract: Results of the study of the lateral surface of single-crystal (SC) sapphire fibers grown along crystallographic directions [0001] and $[11\bar{2}0]$ by the LHPG method are presented. The appearance or absence of faceting of the lateral surface of the fibers depending on the growth direction is analyzed. The crystallographic orientation of the facets is investigated. The microstructure of the samples is investigated with the help of an optical microscope and a JSM-5910LV scanning electronic microscope (JEOL). The crystallographic orientations of the facets on the SC sapphire fiber surface are determined by electron backscatter diffraction (EBSD). The seed orientation is studied by means of XRD techniques.

Keywords: A2. Laser heated pedestal growth; A1. Characterization; B1. Sapphire

1. Introduction

Single-crystal (SC) fibers attracted considerable interest very long ago, in the beginning of the 20th century; however, new opportunities for SC research were opened up by a paper [1] devoted to pulling sapphire fibers from the melt. Thereafter, intensive study resulted in the creation of well-developed growth methods to give rise to practical application [2,3]. Sapphire fibers are recognized for their remarkable characteristics, such as low defect density, high transmission in the near and mid-infrared ranges [4,5] and possibility acting as a crystal host for the creation of light sources [6]. In recent years, interest has arisen in using faceted SC fibers as substrates for drawing semiconductor or superconducting material [7,8] or for sensor applications [9,10]. For different kinds of high-quality crystal fiber devices, the concentration level of the dopants and unwanted impurities as well as faceting of the lateral side should be thoroughly studied and optimized. Therefore, the understanding of growth conditions, including the seed orientation, is critical for growing a crystal fiber optimized for a certain application.

In most cases the occurrence of faceting of grown up crystal fibers is undesirable (Mid-IR radiation delivery, laser action); however, in some cases, on the contrary, it is necessary to achieve the appearance of a certain facet with a flat surface (sensor application). The facets' appearance during crystal growth is natural due to an anisotropic surface free energy tendency to define equilibrium shape corresponding to the minimum value of the surface energy. Actually, the faceting of the crystals may be suppressed by the growth conditions. The problem of facet occurrence on grown crystal fibers has been investigated repeatedly for various methods and conditions of crystal growth. The melt growth crystal fiber

techniques may be classified in the following two main categories: (1) micro floating zone methods; and (2) pulling techniques from a shaper. In all SC fiber growth techniques, an important role is played by the capillary phenomena [11,12]. Facet appearance on the lateral surface of SC fibers was observed while using different growth techniques. At the same time different explanations were provided for SC fiber faceting: (1) influence of manufacturing accuracy of the shaper in μ-PD (micro-pulling-down) technique [13]; (2) seed misalignment [14]; (3) fluctuations of the pulling rate, heating temperature and feed velocity [12,15]. The modeling of the time-dependent behavior of SC fiber growth in an LHPG arrangement [15] demonstrates that the Marangoni convection in the LHPG melting zone could change the growth angle, leading to diameter fluctuations of the growing fiber and thereby to the chance of facet appearance. Nevertheless, there is a lack of systematic study of this effect.

In [16], when growing cylindrical crystals by the Stepanov method (the kind of the shaped crystal growth), various crystal facets were observed on the rod's lateral surface and an attempt was made to explain the facets' appearance and width based on the surface energy influence. Earlier in [17], in the process of sapphire ribbon growth by the Stepanov method, it was found that during seed alignment with an accuracy of several minutes of arc (arcmin), it is possible to obtain smooth facets, some square centimeters in size, on the sapphire ribbon surface. However, there arose growth steps on the ribbon surface, which were formed owing to residual seed misalignment and minor alterations of the growth process conditions. When sapphire ribbon is grown in such a way that the lateral surface is flat (or smooth) face *c* (1000), the steps consist of two quite distinguishable parts—flat facet *c* (1000) and a surface with a rounded (an essentially round) shape. Microscopic analysis of this rounded surface shows [18] that it consists of micro-steps too. In [19], a detailed analysis of the occurrence and shape of the steps depending on the seed misalignment angle relative to the pulling direction was carried out. As a result, a hysteresis characteristic of the dependence of the inclination angle of the ribbon lateral surface on the tangent angle to a meniscus at the triple point was found.

Although the processes accompanying the growth of shaped crystals and SC fibers are similar, fabrication of SC fibers occurs in the conditions of a much stronger influence from the capillary phenomena owing to the smaller sizes of a fiber in comparison with those of a shaped crystal. In our paper, research results regarding the faceting of SC sapphire fibers in the growing process along different crystallographic orientations are presented. The goal was to investigate the occurrence or absence of a facet depending on the growth direction.

2. Experimental

We used an experimental set-up based on the laser heated pedestal growth (LHPG) technique [20–22], which enabled us to grow single crystal fibers with a diameter of about 400–800 μm and a length of up to 25 cm [22]. The fiber was pulled by an oriented seed crystal from the molten tip (pedestal) of the source rod (Figure 1).

For the source rod, single crystals, square shaped in cross-section, with smoothed edges were used. The source rod sizes were 1.3 × 1.3 mm. They were cut from commercially available single crystal (Techsapphire Ltd., Belgorod, Russia). The source crystal was heated by a CO_2 laser (λ = 10.6 μm). The diameter of a molten zone smoothly varied from the source rod to the fiber being grown. The overall dimensions of the molten zone were about ∅1.3 × 1.5 mm. By a special diffractive optical element [23] and a parabolic mirror, the laser radiation spatial distribution was formed as a hollow cone, the cone vertex falling onto the tip of the source rod. This cone meets the surface being heated at a ring strip with the heating area width of about 200 μm. The seed rod was further dipped into the melt and then was pulled up to form an SC fiber. The growth of SC sapphire fibers was done in air.

The facets and the crystallographic axes of sapphire crystals may have different notation in different papers and in some countries. To avoid misunderstanding, we will be using the most widespread literal symbols for the facets: *c* (0001), *a* {11$\bar{2}$0}, and *r* {1011} (Figure 2). Also, the following

notations will be used for the crystallographic orientations: [0001], [11$\bar{2}$0] and [1011] for *C*, *A* and *r* directions, respectively [24]. Both alphabetic and digital notation will be used.

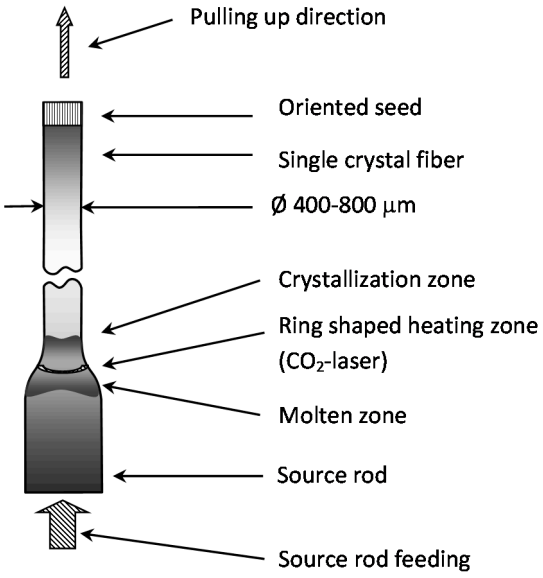

Figure 1. Schematic of experimental set-up. The pulling of the fiber is directed from the bottom upwards.

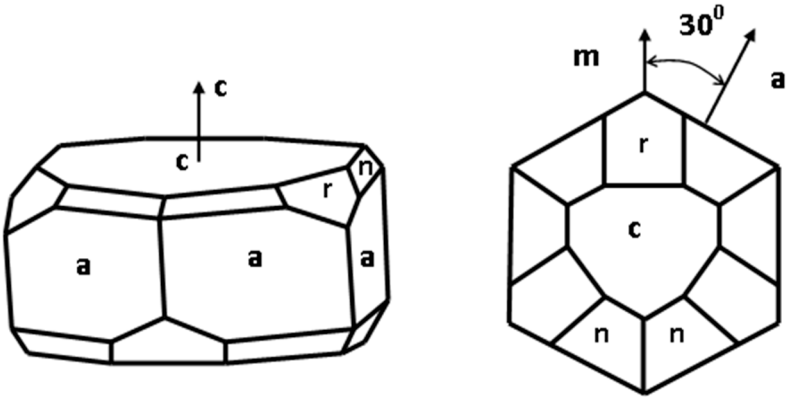

Figure 2. Crystallographic diagram of sapphire.

Crystal fibers were grown along crystallographic orientations [0001] and [11$\bar{2}$0] (perpendicular to planes *c* and *a*, accordingly, [24]). Accuracy of seed preparation along the chosen direction was no worse than 5–6′ (arcmin). The seed orientation relative to the fiber pulling direction was adjusted to within 15–17′ directly in the growth chamber. During the growth, various diameter reduction ratios were obtained by controlling the fiber-drawing speed, according to the mass conservation. The pulling speed amounted to 0.7–3 mm/min for different directions. Although sapphire crystal fibers can be grown up without cracking with a pulling speed of up to 10 cm/min, at a growth rate above 1 cm/min, voids and bubbles, 1 μm in size, were observed in the fibers [25,26]. The probability of bubbles formation depends on a number of different factors. In some experiments voids and bubbles capture was observed at lower pulling rate [27,28], but our experience demonstrated that it is possible to grow high optical quality sapphire fibers even at 2 cm/min pulling rate with the use of a high-quality single crystal source rod. Therefore, we chose the pulling speeds at which high

optical quality was ensured. The fiber cross-section was basically circular, the diameter being about 400–800 μm in different experiments.

The microstructure of the samples was investigated with the help of a JSM-5910LV scanning electron microscope (JEOL). The crystallographic orientations of the facets on the SC fiber surface were determined by the electron backscatter diffraction (EBSD) using a CRYSTAL attachment (Oxford Instruments, Highwycomb, UK). The seed orientations were studied by means of the XRD techniques (D8 DISCOVER and D2 Phaser, Bruker, Karlsruhe, Germany). One of the results is shown in Figure 3 for the seed oriented along *c*-axis.

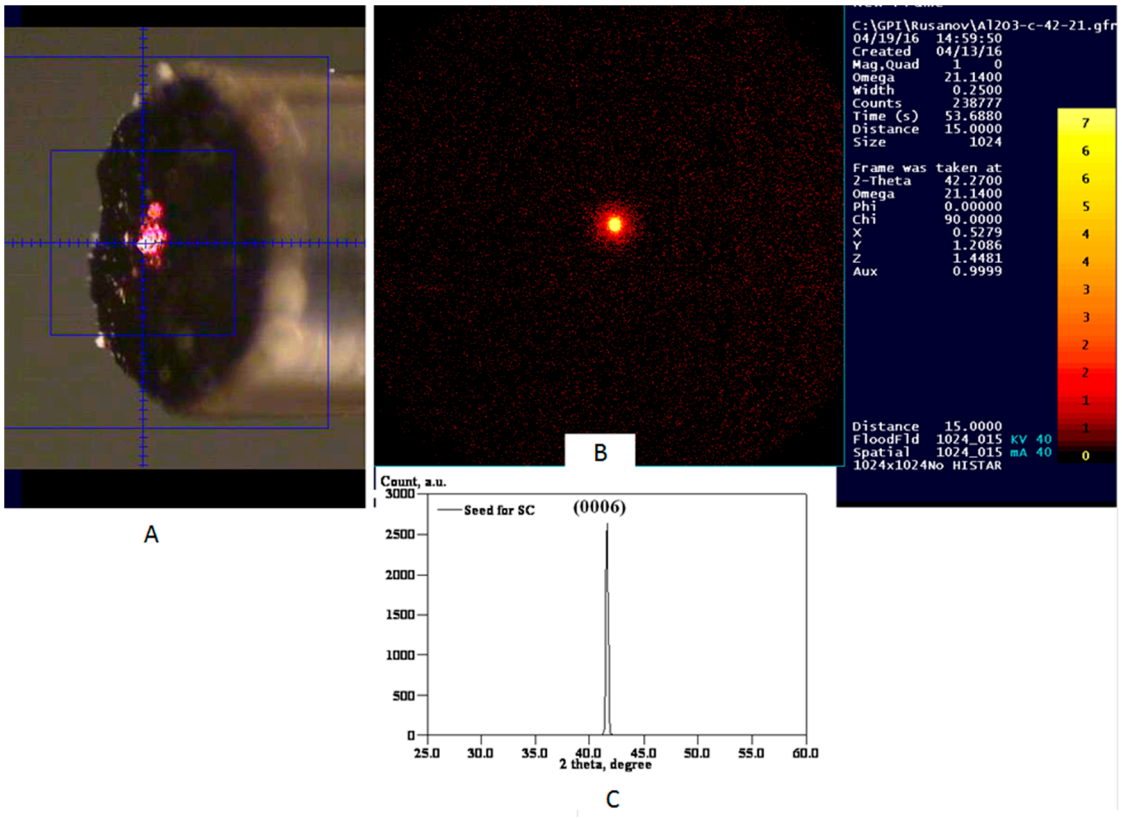

Figure 3. Determination of the seed orientation by means of the XRD techniques: (**a**) Positioning on X-ray beam on samples area by means laser-video system; (**b**) scan frame; (**c**) XRD pattern.

It is clearly seen from the Figure 3 that there is only one reflection spot (0006). The value of experimental diffraction angle 2Θ = 41.62° is very near to the known value 2Θ = 41.678° (Joint Committee on Powder Diffraction Standards (JCPDS) database, Card No. 82-1468 for Al_2O_3).

3. Experimental Results

First of all, sapphire fibers grown along axis [0001] (*C*-axis) were investigated, because this direction is the most important one for the creation of sensors and optical fibers for laser radiation delivery in the mid-IR range.

When the seed orientation was accurately set relative to the normal to the basal plane (accuracy of up to 5′) and relative to the SC fiber growth direction (accuracy of about 17′), at a pulling speed of 0.7 mm/min, the sapphire SC fibers obtained had a slightly round-off cross-section (Figure 4A) without noticeable faceting on the lateral fiber surface (Figure 4B). Nevertheless, micro-facets were observed on this surface. The structure possessed a period of about 5–10 μm (Figure 4C). A similar structure of a lateral surface was observed by many researchers in virtually all SC fibers grown. It is obvious that such a small-scale structure on the fiber surface has a deleterious effect, because it leads

to a loss increase in the light delivery systems. In some cases, it is possible to suppress the micro-facets on the SC lateral surface. For example, in [29], small-scale faceting of the lateral surface of a Cr^{4+}:YAG SC fiber was suppressed at 15° seed orientation from plane (100) towards plane (110).

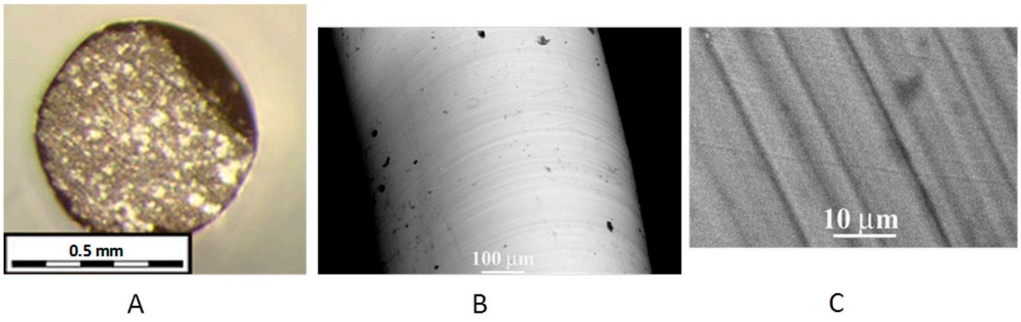

Figure 4. Optical (**A**) and SEM photographs (**B**,**C**) of an SC sapphire fiber grown up along axis [0001] at the precise seed orientation. Photographs demonstrate a slightly rounded-off cross-section (**A**); the absence of large facets, but the presence of micro-facets on the lateral surface (**B**); and the period of the small-scale faceting of the lateral surface (**C**).

The LHPG method ensures steady growth of SC fibers along the *C*-direction without facet appearance on the lateral fiber surface even in conditions of tangible seed misalignment (up to 1°–1.5°) relative to the normal to the basal plane (0001) and the asymmetry of the heating zone. Even in such adverse conditions, one still obtains an approximately round cross-section of the fiber and the absence of appreciable facets on the lateral surface.

To observe facet appearance, seeds with a misalignment angle of ~2.5° and ~7° were used. At 2.5° seed misalignment relative to the normal to the basal plane (0001), facets were observed (Figure 5A) on the lateral side of a fiber with a diameter of about 700 µm.

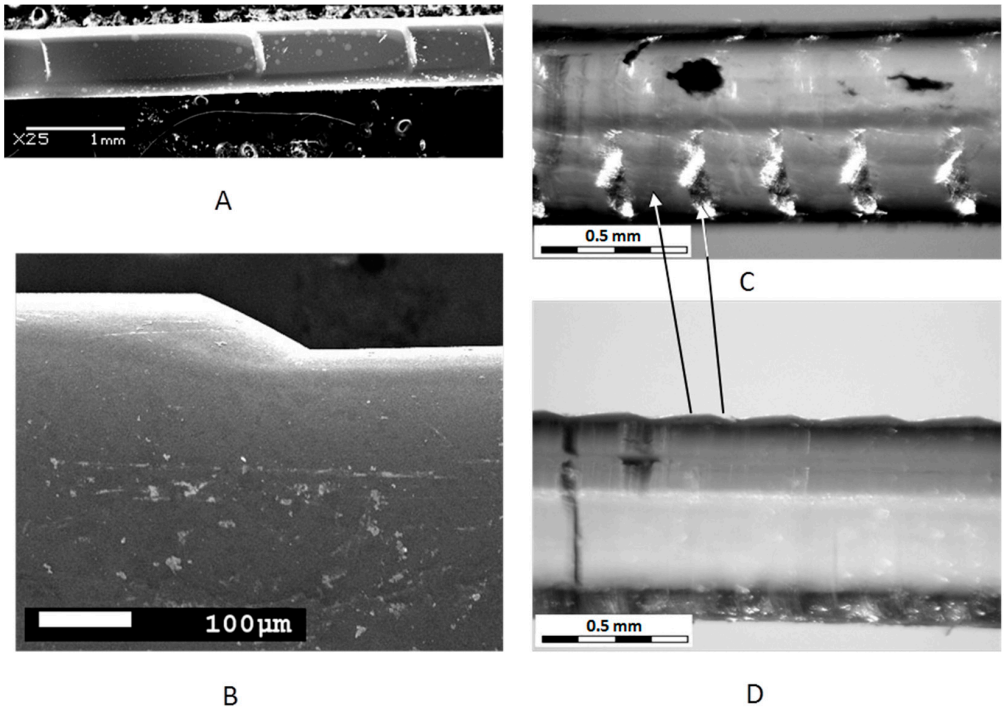

Figure 5. Z-contrast SEM image (**A**,**B**) and optical photographs (**C**,**D**) of an SC sapphire fiber grown up along axis [0001] at different seed misalignment: $\Delta\alpha_1 \approx 2.5°$ (**A**,**B**); $\Delta\alpha_2 \approx 7°$ (**C**,**D**).

Facets arise only on one side of the fiber lateral surface and possess the shape of a boat with a rounded forward part and a flat termination. The length of the steps (flat face $(11\bar{2}0)$) was in the range of about 0.5 mm to 1.5 mm with the absence of any periodicity. The length of the rounded region was much less than the facet length. No facets were observed in the rounded part of steps (Figure 5B). The facets' $(11\bar{2}0)$ growth angle relative to the pulling direction was determined from 5 facets to amount to $\alpha_1 = 2.7 \pm 0.2^\circ \approx \Delta\alpha_1$.

When there was a great seed misalignment ($\Delta\alpha \approx 7^\circ$), a facet on the lateral surface of a fiber, about 880 μm in diameter, was also observed (Figure 5C). The facet was also formed only on one side of the fiber and had the shape of a boat. The flat part of *a*-face $(11\bar{2}0)$ in this case was of comparable length with the rounded part. The pattern of the lateral surface faceting looked like as a sequence of "notches" (Figure 4C) and had a nearly constant spacing between the notches. The facets $(11\bar{2}0)$ growth angle relative to the pulling direction was determined from 6 facets and amounted to $\alpha_2 = 6.8 \pm 0.5^\circ \approx \Delta\alpha_2$. The height of the steps proved to be $h_2 = 34 \pm 3$ μm for $\Delta\alpha_2 \approx 7^\circ$ and $h_1 = 68 \pm 5$ μm for $\Delta\alpha_1 \approx 2.5^\circ$.

The appearance of small-scale facets on the SC fiber lateral surface at both the misalignment angles was not revealed, in contrast to the case of fiber growing with a precisely oriented seed.

It is necessary to note that the faceting pattern depended on the misalignment angle only and was well reproduced in different experiments with the same angle.

The SC sapphire fibers grown along direction $[11\bar{2}0]$ (*A*-axis) are of interest, because the basal *c*-facets and rhombohedron facets $\{h0\bar{h}l\}$ may appear in this orientation as flat faces. In this case, the basic morphological rhombohedron {1011} ([24]) is most interesting, because the *r*-plane is necessary, for example, for the creation of superconducting structures [7]. Besides, it was possible to compare experimentally the growth of *c*- and *r*-facets. For this growth direction, both faces are oriented along the lateral surface of the SC fiber and are in identical capillary and thermal conditions in the ideal case. In the experiment, the seeds orientated along axis $(11\bar{2}0)$ with an accuracy of $6'$ were used. The seed orientation accuracy in the growth chamber was about $17'$ (without reference to planes *c* and *r*). The pulling speed was 1.4 mm/min.

In all experiments, one-side faceting of the SC fiber lateral surface was observed. However, the view of the facet varied from experiment to experiment and sometimes even in the course of one growth process. In all cases, the facet shape was boat-like with variations in the beginning of the facet growth.

In one experiment, short steps with flat planes with the height $h = 35 \pm 4$ μm and with the length of about 0.2–0.4 mm were observed (Figure 6A, an SC fiber with a diameter of 820 μm). The steps were similar to *c*-facets (0001) arising at a big seed misalignment angle (Figure 5C,D). It is interesting to note that the usually rounded part arising before the facet growth was faceted in this case (Figure 6B). It was impossible for us to identify all the faces shown because of the small sizes of the objects. Also, additional experiments are necessary to identify the crucial physical factor for facet appearance or suppression in the beginning of facet growth.

In another experiment (Figure 7A, an SC fiber with a diameter of 760 μm), long-length facets (from 0.5 mm to 1.5 mm) on the lateral surface were observed with the usual rounded (not faceted) part in the beginning of growth of the long facet and with a flat face with a smooth surface. This facet was identified by the EBSD method as basal *c*-plane (0001) (Figure 7B,C). The polar figure computed by the JEOL software (Figure 7C) demonstrates that the facet corresponds to *c*-plane (0001). The deviation of the normal to this plane away from the growth direction is less than 10° (the point in the left corner of the figure).

In Figure 7B, the step structure of the rounded part of facet (0001) is quite visible. It is also seen that the step growth transforms into the flat surface of a facet. No faceting is observed on the rounded part of the step.

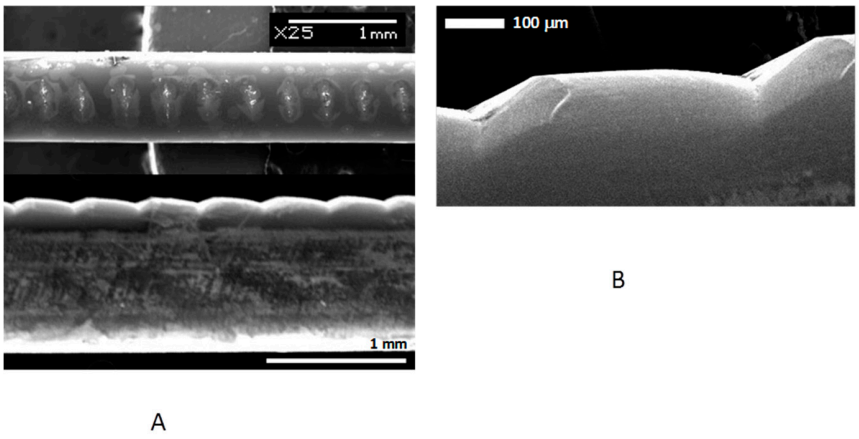

Figure 6. SEM image of an SC sapphire fiber grown along axis [11$\bar{2}$0] (**A**) general view; (**B**) the view of one of the steps.

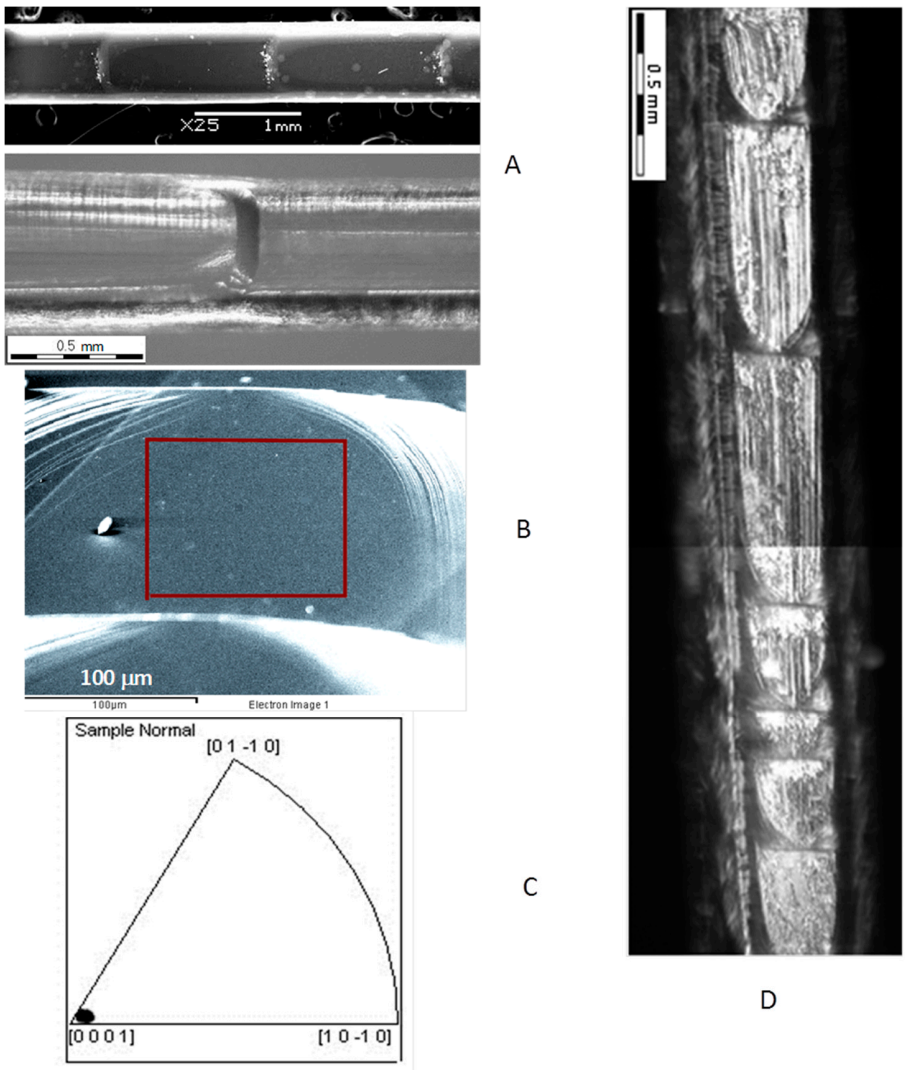

Figure 7. Optical microphotograph (**A** bottom, **D**) and SEM image (**B**) of a sapphire SC fiber grown along axis [11$\bar{2}$0]: (**A**) general view of flat faces; (**B**) SEM image of one of the flat planes, with the region of the EBSD-measurement pointed out by a rectangle; (**C**) polar figure after JSM-5910LV (JEOL) software; (**D**) general view of the defected faces (combination of several photos along the sapphire fiber).

In the presence of power fluctuations of the heating laser (temperature fluctuations in the melt zone), the facets on the fiber lateral surface were rough (Figure 7D, an SC fiber with a diameter of 615 μm) and strongly varied in length. The defects visible in the photographs show that the growth process was unstable. The growth steps can be easily seen on the surface of the rounded part.

In the third group of experiments (Figure 8A, a sapphire fiber, 570 μm in diameter,) unilateral appearance of facets with a smooth surface and a long length is observed on the lateral fiber surface. The view of the facets did not differ from those shown in Figure 7A. However, the EBSD measurements showed that this face is the *r*-plane. In Figure 8B, the microstructure of the flat face surface demonstrating the absence of defects and the presence of lines of the layer-wise growth are shown. In the central part of the facet, the lines are circular and become virtually straight near the facet edges. Also the step growth transforms into the flat surface of a facet (Figure 8C).

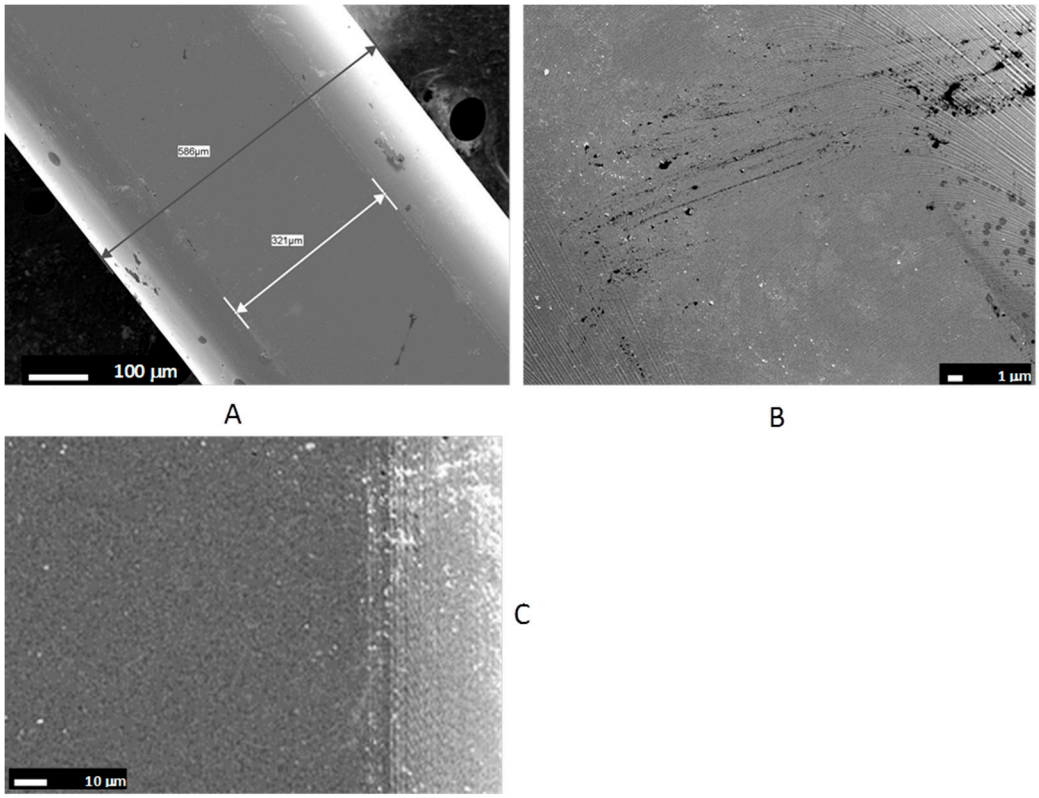

Figure 8. SEM image of a sapphire SC fiber grown along axis [11$\bar{2}$0]: (**A**) general view of one of the facets (*r*-plane); (**B**) microstructure of the central part of the facet; (**C**) growth steps near the boundary of the flat face.

It is necessary to note that in all cases of faceting observation on the SC fiber lateral surface, the facets consisted of separate smooth or rough regions separated by bow-shaped or faceted steps, the convex part of the steps being co-directed with the fiber pulling direction. A rough surface of the facets revealed in some cases was a consequence of unstable growth conditions. The appearance of small-scale faceting of the lateral surface of SC fibers was not revealed.

4. Discussion

The above results of the research of faceting of the lateral surface of sapphire SC fibers show that the occurrence of faces on the lateral surface of such fibers is a natural phenomenon, as the faceting probability in growing fibers along different crystallographic directions is different.

Only unilateral faceting of SC fibers was observed regardless of the shape of the seed (flat, oriented along the crystallographic axes, or cone-shaped). At the same time, in [7], bilateral faceting of a sapphire fiber was obtained using a specially prepared seed. It is possible that the difference in the shape of the SC fibers is associated with the difference in symmetry of the thermal zone.

The surface of the smooth faces was found to contain growth layers, the central part being, in most cases, absolutely smooth. At the edges of faces, near the transition to a rounded part of the face and to the rounded lateral surface of a fiber, growth steps are quite visible (Figures 6B, 7D and 8C). Unfortunately, we did not investigate the surface microstructure of the smooth faces (see for example [30,31]).

In the case of temperature fluctuations in the melt zone, layer-wise growth transforms into non-uniform lateral or normal growth of a facet, which leads to clear-cut defects and roughness of the facet. In experiments we did not monitor the temperature in the melting zone, but rather the heating power. The typical stability of the heating power was $\pm$5%. Operation in this mode resulted in obtaining SC sapphire fibers with small diameter variations (less than 2%) and smooth facet faces. The growth process with heating power stability of about 10% led to diameter variations ~5% and roughness of the facets. It should be noted that even in this case, sapphire crystal fibers may be grown with smooth or faceted lateral surfaces, depending only on the seed orientation accuracy.

In growing a SC fiber along direction [0001], the formation of facets (11$\bar{2}$0) (*a*-planes) on the lateral surface can be suppressed by choosing the precise seed orientation with respect to the growth direction. However, in this case, small-scale faceting on the surface can arise, which increases the optical loss in the fiber employed for radiation delivery. At precise seed orientation along direction [0001], the heating power variation in the range of $\pm$10% results in small diameter variation (about 3%–5%), but it does not produce facet formation. When the seed is misaligned by more than 1.5°–2°, facets appear on the lateral surface of the fiber, of which the growth angle corresponds sufficiently precisely to the seed misalignment angle. At small seed misalignment angles, the *a*-facets turn out to be smooth and long (up to 1–1.5 mm). At large misalignment angles, the facet length sharply decreases (down to 0.3 mm), as does the length of the smooth part. In the case of a misaligned seed, small-scale faceting on the lateral surface is not observed.

Growth of SC sapphire fibers along direction [11$\bar{2}$0] (*A*-axis) shows essentially less certain character of the facet appearance on the lateral surface.

First, the value of the facet growth angle relative to the growth direction is not related to the seed misalignment angle. The maximal possible angle of the deviation of the seed orientation with respect to the growth direction is less than 30′. This value allows for the accuracy of seed cutting, the accuracy of the cone formation at the seed end, and the accuracy of the seed orientation in the growth chamber. Thus, the facet appearance angle can amount to 1°–2° with respect to the pulling direction in the case of short facets and to 0.5°–1° in the case of long facets.

Second, because manifestation of the *c*- and *r*-planes is possible at the seed orientation along the *A*-axis, a question arises as to the priority of the growth of this or that facet on the lateral fiber surface and as to the mechanisms underlying this priority. The Wulff principle of surface energy minimum [32] indicates that the size of a crystal facet is inversely proportional to the value of the specific surface energy of this facet. In case of an SC fiber, only unilateral faceting on the lateral surface is observed, i.e., the value of surface energy defines the formation probability of this facet. The analysis of the value of surface energy of different crystallographic planes performed according to different theoretical models yields quite different values [33–36]. At the same time, the experimental results of [16] showed a quite certain sequence of the width of the facets appearing on the lateral surface of a cylindrical crystal grown by the Stepanov method. This sequence is $c > r > a$, and an approximate relationship of the facet width can be written out as 8:4:1.

If one considers the above relationship of the facet width as the relationship of the appearance probability of this or that facet, the probability of the occurrence of an *r*-facet proves to be less than

that of an *a*-facet. Nevertheless, it was an *r*-facet that appeared in a number of experiments, although its occurrence was much rare than that of an *a*-facet.

Thus, one may assume that the main factor controlling the appearance of any facet on the lateral surface of an SC fiber in growing the fiber along *a*-axis is accidental fluctuation of the melt temperature leading to variation of the conditions at the growth front.

The mechanism of facet formation on the lateral surface of an SC fiber is well described by the model proposed in [19] for the case of sapphire ribbon. According to this model [19], the condition of constancy of the growth angle asserts only in the stage of transition growth (formation of the rounded part of the step). During the growth of the faceted parts, the shape of the melt meniscus is defined only by its height and by the sapphire SC fiber diameter at the given point. The distinction of our case consists in the presence of axial symmetry of the thermal field, which leads to a distinction in the initial stage of facet growth: in the formation of the rounded part and in the beginning of the flat facet growth. Otherwise, the mechanism proposed describes the facet growth well to show the dependence of the critical inclination angle of the tangent at the triple point on the angle of facet appearance at a constant temperature. As the melt temperature changes, the critical angle can also change, leading to facet shortening or lengthening.

5. Conclusions

The experiments on growth of sapphire SC fibers by the LHPG method along crystallographic directions [0001] and [11$\bar{2}$0] pointed to the strong influence of anisotropy of the surface energy and thermal conditions on facet formation on a lateral fiber surface. High stability of the melt temperature opens up the possibility of obtaining smooth faces *c* (0001), *a* {11$\bar{2}$0} and *r* {1011}. The faceting probability of a sapphire fiber grown along the *a*-axis is defined by anisotropy of the surface energy and by melt temperature fluctuations. Temperature instability also leads to non-uniform lateral or normal facet growth instead of layer-wise growth and, as a consequence, to defects and surface roughness. Facets have been found to have a complex structure. The smooth central part is replaced by steps at the cylindrical surface boundary of the fiber and in the region of transition growth. Axial symmetry of the thermal field leads to a complex shape of the initial rounded part and of the region of the beginning of the facet formation.

Acknowledgments: The research was supported by the Russian Academy of Sciences in the framework of the Program for Basic Research "Supersensitive sensors and huge strengthening of the fields by optical metamaterials".

Author Contributions: Liudmila D. Iskhakova and Sergey V. Lavrishchev performed the experiments with the electron microscope including surface image of the crystal fibers and EBSD measurements. Also, they performed XRD measurements of seed orientation. Vitalii V. Kashin and Sergey Ya. Rusanov performed the experiments with crystal fiber growth. Vladimir F. Seregin performed the experiments with an optical microscope, including the measurements of growth angles of the facets. Vladimir B. Tsvetkov conceived the experiments, performed the analysis of experimental results and wrote the paper.

Conflicts of Interest: The authors declare no conflict of interest.

References

1. Labelle, H.E., Jr.; Mlavsky, A.I. Growth of sapphire filaments from the melt. *Nature* **1967**, *216*, 574–575. [CrossRef]
2. Haggerty, J.S. *Production of Fibers by a Floating Zone Fiber Drawing Technique*; Final Rep. NASA-CR-120948; NASA: Greenbelt, MD, USA, 1972.
3. Feigelson, R.S. Growth of Single Crystal Fibers. *MRS Bull.* **1988**, *13*, 47–55. [CrossRef]
4. Nubling, R.K.; Harrington, J.A. Single-crystal laser-heated pedestal-growth sapphire fibers for Er:YAG laser power delivery. *Appl. Opt.* **1998**, *37*, 4777–4781. [CrossRef] [PubMed]
5. Jundt, D.H.; Fejer, M.M.; Byer, R.L. Growth and optical properties of single-crystal fibers. *SPIE Infrared Fiber Opt.* **1989**, *1048*, 39–43.

6. Lai, C.-C.; Cheng, N.-C.; Wang, C.-K.; Tjiu, J.-W.; Lin, M.-Y.; Huang, S.-Y. Simple and efficient defect-tailored fiber-based UV-VIS broadband white light generation. *Opt. Express* **2013**, *21*, 14606–14617. [CrossRef] [PubMed]
7. Xu, Y.; Djeu, N.; Qian, Z.; Xu, Z.; He, P. Bhattacharya Rabi. $YBa_2Cu_3O_{7-\delta}$ Films Grown on Faceted Sapphire Fiber. *IEEE Trans. Appl. Superconduct.* **2011**, *21*, 3281–3284. [CrossRef]
8. Snigirev, O.; Chukharkin, M.; Porokhov, N.; Rusanov, S.Y.; Kashin, V.V.; Tsvetkov, V.B.; Kalabukhov, A.; Winkler, D. Pulsed Laser Deposition of Thin YBCO Films on Faceted YSZ Single Crystal Fibers. *J. Phys. Conf. Ser.* **2014**, *507*, 022033. [CrossRef]
9. Zhang, Y.; Pickrell, G.R.; Bing, Q.; Safaai-Jazi, A.; Wang, A. Single-crystal Sapphire Based Optical Polarimetric Sensor for High Temperature Measurement. *Sensors* **2006**, *6*, 823–834. [CrossRef]
10. Bufetova, G.A.; Kashin, V.V.; Nikolaev, D.A.; Papin, Y.M.; Rusanov, S.Y.; Shcherbakov, I.A.; Seregin, V.F.; Tsvetkov, V.B.; Yakovlev, A.A. Zonal doped crystal fibers for temperature measurements. *Laser Phys. Lett.* **2007**, *4*, 440–443. [CrossRef]
11. Ciszek, T.F.; Schwuttke, G.H.; Yang, K.H. Factors influencing surface quality and impurity distribution in silicon ribbons grown by the capillary action shaping technique (CAST). *J. Cryst. Growth* **1980**, *50*, 160–174. [CrossRef]
12. Rudolph, P.; Fukuda, T. Fiber Crystal Growth from the Melt. *Cryst. Res. Technol.* **1999**, *34*, 3–40. [CrossRef]
13. Klejch, M.; Němec, M.; Kubát, J.; Polák, J. Preparation, properties and application of sapphire single-crystal fibers grown by the EFG method. *EPJ Web Conf.* **2013**, *48*, 00007. [CrossRef]
14. Pollock, J.T.A.; Bailey, J.S. Fracture strength in tension of a-axis filamentary sapphire grown by EFG. *J. Mater. Sci.* **1974**, *9*, 510–512. [CrossRef]
15. Young, G.W.; Heminger, J.A. Modeling the time-dependent growth of single-crystal fibers. *J. Cryst. Growth* **1997**, *178*, 410–421. [CrossRef]
16. Nosov, Y.G.; Bakholdin, S.I.; Krymov, V.M. Faceting of Sapphire Crystals Grown from a Melt by the Stepanov Method. *Tech. Phys.* **2009**, *54*, 239–245. [CrossRef]
17. Antonov, P.I.; Krymov, V.M.; Nosov, Y.G.; Shulpina, I.L. Growth of Basal Facet Ribbon Sapphire Crystals and Study of Their Dislocation Structure. Proceedings of the Conference "Shaped Crystal Growth by Stepanov Method, Plasticity and Strength of Crystals", St. Petersburg, Russia, 22–24 October. *Bull. Russ. Acad. Sci. Phys.* **2004**, *68*, 880–884.
18. Nosov, Y.G.; Bakholdin, S.I.; Krymov, V.M.; Zamoryanskaya, M.V.; Kolesnikova, E.V.; Domracheva, Y.V. Fine structure of faces and imperfections of surface layers of shaped sapphire crystals. *Bull. Russ. Acad. Sci. Phys.* **2009**, *73*, 1349–1354. [CrossRef]
19. Asryan, A.A.; Rossolenko, S.N.; Kurlov, V.N.; Krymov, V.M. Analysis of the features of Meniscus profile curves during growth of base-faceted sapphire ribbons. *Bull. Russ. Acad. Sci. Phys.* **2009**, *73*, 1333–1337. [CrossRef]
20. Fejer, M.M.; Nightingale, J.L.; Magel, G.A.; Byer, R.L. Laser-heated miniature pedestal growth apparatus for single-crystal optical fibers. *Rev. Sci. Instrum.* **1984**, *55*, 1791–1796. [CrossRef]
21. Feigelson, R.S. Pulling optical fibers. *J. Cryst. Growth* **1986**, *79*, 669–680. [CrossRef]
22. Bufetova, G.A.; Kashin, V.V.; Nikolaev, D.A.; Rusanov, S.Y.; Seregin, V.F.; Tsvetkov, V.B.; Shcherbakov, I.A.; Yakovlev, A.A. Neodymium-doped graded-index single-crystal fibre lasers. *Quantum Electron.* **2006**, *36*, 616–619. [CrossRef]
23. Kazanskiy, N.L.; Kotlyar, V.V.; Soifer, V.A. Computer-aided design of diffractive optical elements. *Opt. Eng.* **1994**, *33*, 3156–3166.
24. *Ruby & Sapphire: A Coll. Book*; Klassen-Neklyudova, M.V., Bagdasarov, K.S., Eds.; Nauka: Moscow, Russia, 1974; pp. 47–59.
25. Pollock, J.T.A. Filamentary sapphire. Part 1. Growth and microstructural characterization. *J. Mater. Sci.* **1972**, *7*, 631–648. [CrossRef]
26. Merberg, G.N.; Harrington, J.A. Optical and mechanical properties of single-crystal sapphire optical fibers. *Appl. Opt.* **1993**, *32*, 3201–3209. [CrossRef] [PubMed]
27. Ghezal, E.A.; Nehari, A.; Lebbou, K.; Duffar, T. Observation of Gas Bubble Incorporation during Micropulling-Down Growth of Sapphire. *Cryst. Growth Des.* **2012**, *12*, 5715–5719. [CrossRef]
28. Bunoiu, O.M.; Duffar, T.; Nicoara, I. Gas bubbles in shaped sapphire. *Prog. Cryst. Growth Charact. Mater.* **2010**, *56*, 123–145. [CrossRef]

29. Ishibashi, S.; Naganuma, K.; Yokohoma, I. Cr, Ca: $Y_3Al_5O_{12}$ laser crystal grown by the laser-heated pedestal growth method. *J. Cryst. Growth* **1998**, *183*, 614–621. [CrossRef]
30. Cuccureddu, F.; Murphy, S.; Shvets, I.V.; Porcu, M.; Zandbergen, H.W.; Sidorovic, N.S.; Bozhko, S.I. Surface morphology of c-plane sapphire (α-alumina) produced by high temperature anneal. *Surf. Sci.* **2010**, *604*, 1294–1314. [CrossRef]
31. Becker, T.; Birkner, A.; Witte, G.; Woell, C. Microstructure of the α-Al_2O_3 $(11\bar{2}0)$ Surface. *Phys. Rev. B* **2002**, *65*, 115401. [CrossRef]
32. Wulff, G. Zur Frage der Geschwindigkeit des Wachstums und der Aufloesung der Kristallflaechen. *Z. Kryst. Mineral.* **1901**, *34*, 449–530.
33. Dobrovinskaya, E.R.; Lytvynov, L.A.; Pishchik, V. *Sapphire: Material, Manufacturing, Applications*; Springer Science+Business Media: New York, NY, USA, 2009; pp. 55–80.
34. Mackrodt, W.C.; Davey, R.J.; Black, S.N.; Docherty, R. The morphology of α-Al_2O_3 and α-Fe_2O_3: The importance of Surface relaxation. *J. Cryst. Growth.* **1987**, *80*, 441–446. [CrossRef]
35. Gay, D.H.; Rohl, A.L. MARVIN: A New Computer Code for Studying Surfaces and Interfaces and Its Application to Calculating the Crystal Morphologies of Corundum and Zircon. *J. Chem. Soc. Faraday Trans.* **1995**, *91*, 925–936. [CrossRef]
36. Bakholdin, S.I.; Maslov, V.N. Simulation of surface energies of sapphire crystals. *Phys. Solid-State* **2015**, *57*, 1213–1219. [CrossRef]